Article

Not peer-reviewed version

Rapid Thermal Processing of Kesterite thin films

Maxim Ganchev * , Stanka Spasova * , Taavi Raadik , Arvo Mere , Mare Altosaar , Enn Mellikov

Posted Date: 3 July 2023

doi: 10.20944/preprints202306.2134.v1

Keywords: photovoltaics, multinary chalcogenides, thermal annealing; Kesterite, XRD

Preprints (www.preprints.org) | NOT PEER-REVIEWED | Posted: 3 July 2023 doi:10.20944/preprints202306.2134.v1

Article

Rapid Thermal Processing of Kesterite Thin Films

M.Ganchev [1,2], S.Spasova [2], T.Raadik [1], A.Mere [1], M.Altosaar [1] and E.Melikov [1]

[1] Department of Materials Science, Tallinn University of Technology, 19086 Tallinn, Ehitajate tee 5, Estonia
[2] Central Laboratory of Solar Energy and New Energy Sources – Bulgarian Academy of Sciences, 72 Tzarigradsko shaussee blvd, 1784 Sofia, Bulgaria
* Correspondence: perovskite.psc@gmail.com

Abstract: In this contribution we present work on rapid thermal annealing of as-electrodeposited thin films of Cu_2ZnSnS_4. The treatment was carried out in cold wall tubular reactor in dynamic conditions with variations of temperature, speed and time of the specific elements of the process. The effect of annealing was investigated by X-ray diffractometry, Raman scattering and Scanning Electron Microscopy (SEM). The phase composition of the films in dependence on conditions of treatment was analysed and have been shown that in slow and prolonged high-temperature process the low temperature binaries react completely and only Kesterite and ZnS is left. In addition, structural investigations by XRD have shown gradual decrease of crystallite sizes when the temperature level and duration of the high-temperature segment increases and respectively increase in the strain, due to formation of the phases in non-equilibrium conditions. In opposite, when the speed of dynamic segments in the process decreases the both crystallite size and strain of the Kesterite decreases non-monotonically. The grain sizes of Kesterite, presented by SEM investigations, have shown increase when the temperature and the duration increase, respectively the speed decreases with exemption at higher temperature near 750° C. The set of experiments gave idea by scrupulous analysis of Raman data to elucidate the track for fine manipulating of the defects in the structure of CZTS thin films having in mind the dependences of the ratios of $Q = I_{287}/I_{303}$ and $Q' = I_{338}/(I_{366}+I_{374})$ on the process variables.

Keywords: photovoltaics; multinary chalcogenides; thermal annealing; Kesterite; XRD

1. Introduction

The increased capacity of the worldwide photovoltaics is on the way near the 2030 year to get closer to the needs for zero footprint on the ecology system. Actually, Silicon based solar cells technology dominates the market of photovoltaics with near 95 % of installed modules [1]. Multinary chalcogenides are large class of compounds with special application in photovoltaics. Beginning with chalcopyrite $CuInSe_2$, $Cu(In,Ga)Se_2$, $CuInS_2$ was established a sustainable generation of compounds successfully competing silicon based photovoltaics technologies [2,3] with record efficiencies of 23.4 % for Cd free CIGS device [4] and 26.2% for CIGS based solar cells with electron back reflector [5]. They have several advantages as thickness in nano – to micrometric dimensions, very high absorption coefficient near 105 cm^{-1} and tunable band gap from 1.0 to 1.5 eV depending on kind and ratio of chalcogens. These items encourage the mass production but scarcity of rare earth elements In, Ga limits the perspectives for their application. In an attempt to overcome this obstacle were developed a new class of compounds of Kesterite where the couple In and Ga is replaced with abundant elements Zn and Sn. Similar to Chalcopyrite (CIGSSe), the Kesterite (CZTSSe) have tetragonal crystal structure of Zinc Blende [6]. CZTSSe is a p-type semiconductor with tunable band gap between 1.0 up to 1.5 eV with direct transitions and high absorption coefficient in the range of 104 - 105 cm^{-1}[7,8]. Up to date, the record efficiency of CZTSSe device regardless of the deposition method is 12.6 % reported in 2014 by IBM research group [9]. Despite significant efforts in the years to improve working characteristics of the CZTSSe solar cells there are mentioned several considerable issues on weak performance parameters – deep level defects, narrow phase stability region, non-ideal device architecture. There is an approach for modification of properties of the absorber material by doping or alloying with additional constituents as alkali dopants (Li, Na, K) or isoelectronic substitutions but there were no reports for real improvement [10] and rather effective management of the intrinsic defects is the way for optimization of the optoelectronic properties of the Kesterite absorber materials.

2. Materials and Methods

Substrate layers were deposited electrochemically in potentiostatic conditions using the classic three-electrode cell configuration. Working electrodes were 2 x 1 cm^2 sized tin oxide covered soda lime glasses positioned against platinum gauze and a saturated mercury sulfate (MSE) reference electrode (0.6151 V vs. SHE). Electrolytes for electrodeposition of Cu-Zn-Sn-S layers were 4 M KCNS aqueous solutions of 0.4 M sodium acetate buffer containing totally 9 mM of the chloride salts of Cu^+, Zn^{2+}, $SnSO_4$ and $Na_2S_2O_3$ in related ratio. The composition of the as deposited Cu-Zn-Sn-S layers was copper-poor and zinc – rich with deficiency of sulfur against the stoichiometry. The influence of the substrate on the composition of the layers was estimated as negligible. The process that was set up was described in detail elsewhere [publ25]. Reactive annealing was performed in cold walls quartz tubular reactor under flow of 5% H_2S in N_2 at atmospheric pressure. Temperature profile was controlled in dynamic equilibrium by IR Ulvac-RICO heating system supplied with PC driven controller. The system works under continuous cooling provided by chiller-supplied circulation of working fluid at 10 °C and blowing with 0.6 MPa pressurized air. The heating was done by direct IR irradiation on the length of the reactor with xenon lamps. In these conditions at every segment the process temperatures were differing from set points in values less than 0.1%. Below 220 °C the ramp-down process temperature didn’t follow strictly the set point values but it is believed that reactions here are faded. An example for work temperature profile is shown in Figure 1.

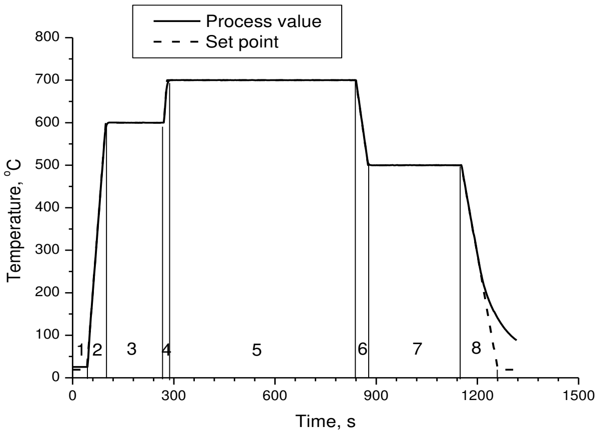

Figure 1. Temperature profile of rapid thermal processing of CZTS films.

The parameters for specific program configuration in details are summarized in Table.1. After work cycle the reactor volume was rinsed by N_2 stream for 5 min.

Scanning electron microscopy and energy dispersive X-ray analysis (EDAX) was performed on Hitachi TM 1000 unit supplied with X-ray source and detector equipment at accelerating voltage of 15.0 kV and acquisition time of 90 sec. The X-ray diffraction (XRD) analysis was performed by a Rigaku Ultima IV diffractometer with Cu-Kα radiation (λ=1.5418Å) at 40 kV accelerating voltage. The diffracted beam was scanned in steps by 0.01 ° for 2 sec in an angular range from 10 to 80 degrees 2Θ.

Table 1. Process parameters of rapid thermal annealing of thin films CZTS.

Probe	**Base**	**Duration**	**Duration**	**Speed fast**	**Speed slow**	**T °C** 750 °C	**T °C** 650 °C	**T °C** 600 °C
Sample	159s1& 150s2	148s4& 159s2	148s1& 151s3	158s1& 157s1	150s1& 161s1	149s1& 161s2	148s3& 149s3	162s1& 160s2
1seg	19°C 10s	19°C 10s	19°C 10s	19°C 10s	19°C 10s	19°C 10s	19°C 10s	19°C 10s
2seg	600°C 1min	600°C 1min	600°C 1min	600°C **30 sec**	600°C **3min**	600°C 1min	600°C 1min	600°C 1min
3seg	600°C 3min	600°C 3min	600°C 3min	600°C 3min	600°C 3min	600°C 3min	600°C 3min	600°C 3min
4seg	700°C 10s	700°C /10s	700°C 10s	700°C **5 s**	700°C **30s**	**750°C** 10s	**650°C** 5 s	**600°C** 5s
5seg	700°C 15min	700°C **10min**	700°C **5min**	700°C 15min	700°C 15min	700°C 15min	700°C 15min	700°C 15min
6seg	500°C 40s	500°C 40s	500°C 40s	500°C **20s**	500°C **2min**	500°C 45s	500°C 15 s	500°C 15s
7seg	500°C 5min	500°C 5min	500°C 5min	500°C 5min	500°C 5min	500°C 5min	500°C 5min	500°C 5min
8seg	19°C 2min	19°C 2min	19°C 2min	19°C 1min	19°C 10min	19°C 2min	19°C 2min	19°C /2min

Qualitative phase analysis was performed on PDXL Rigaku's ICDD PDF2 phase research platform [11]. The room temperature (RT) micro Raman spectra was recorded on Horiba LabRam 800 high-resolution spectrometer equipped with a multichannel detector on backscattering regime. Light source was a red laser with a 633 nm wavelength focused at least on 10 µm spot diameter, providing a spectral resolution of 0.5 cm^{-1}.

3. Results

The reactive annealing is performed in compliance with both suggested reaction path and structural features in [12]. In conformity of the proposed reaction sequence the synthesis and structure formation of CZTS from binaries Cu_2S and SnS_2 trough reaction of Cu_2SnS_3 with ZnS completes at temperatures higher than 600 °C. In this sense the temperature profile configuration is directed onto modification of the part where the direct formation of the quaternary CZTS takes place.

Detailed analysis of results for features of rapid thermal annealing consists of scrupulous phase analysis and assessment of the influence of parameters of annealing process on the crystal cell parameters of the target phase – Kesterite (Cu_2ZnSnS_4). In contrast to Stannite where [13,14] fine difference between some close disposed reflexes of $Cu_2ZnSnSe_4$ and either ZnSe or other binaries could become apparent trough more precise angle-resolved analysis, the case for Kesterite is rather more complicated [15] and additional method as Raman shift is essential for a correct evaluation of phase distribution.

On the Figure 2 are presented XRD patterns of samples 1, 2 and 3 annealed at different durations (15 min, 10 min and 5 min respectively) of the Segment 5 at 700 °C – according to Figure 1.

Preprints (www.preprints.org) | NOT PEER-REVIEWED | Posted: 3 July 2023 doi:10.20944/preprints202306.2134.v1

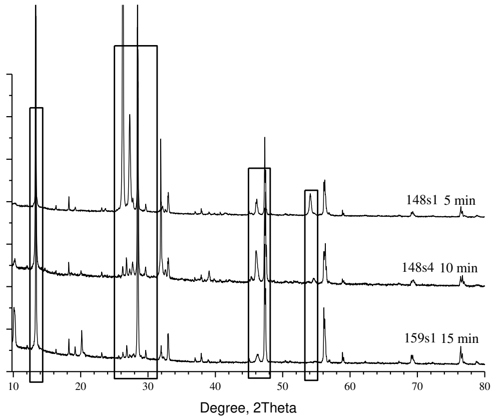

Figure 2. XRD pattern of samples annealed in different duration of Segment 5 (see Figure 1).

The patterns are dominated of characteristic reflexes for the Kesterite phase [1-01-075-4122] at 28.4° (1,1,2), 47.3° (2,2,0) and 56.1° (3,1,2) and its minorities at 16.32°, 18.23°, 23.13°, 29.6°, 32.9°, 36.9°, 37.9°, 40.7°, 44.9°, 56.9°, 58.8°, 67.3°, 69.1°, 76.4° and 78.8° in 2Θ scale. Additional appreciable reflexes are detected near 10.2°, 13.3°, 26.2° 54° and 66.1° and confirm that the system is definitely not monophase. The formal phase analysis performed through [11] and presented in Table.2 have specified for Sample 1-Kesterite, ɑ-SnS [1:01-083-1758]; Cu_7S_4 – [1:00-024-0061] and CuS – [1:03-065-3928].

Table 2. Phase composition according to XRD [11] and Raman shift analyses.

Sample	process	Cu_2ZnSnS_4	ZnS	SnS	CuS	Cu_7S_4	Cu_2S	ZnS	ZnS	ZnS(W)
		Kesterite-4122	h		Covellite	Roxbyite	digenite	h	h	0688h
1-159s1	Base 15min, 700 °C	●+	●$_{2201}$+	◊	◊	◊	◊-	●$_{2424}$	●$_{2195}$	◊
2-148s4	Time-10 min	●+	●$_{2347}$	●+	●	●	◊-	◊	◊	●
3-148s1	Time – 5 min	●+	◊	●+	●	●	◊-	◊	◊	◊
4-158s1	Speed-fast	●+	●$_{4998}$+	●	◊	◊	◊±	◊	◊	◊
5-150s1	Speed-slow	●+	●$_{6022}$+	◊	◊	◊	◊	◊	◊	◊
8-149s1	Temp-750^{o}C	●+	●$_{2140}$	◊-	◊	◊	●$_{9133/-}$	◊	◊	◊
7-148s3	Temp-650^{o}C	●+	●$_{4989}$	●+	◊	◊	◊±	◊	◊	◊
6-162s1	Temp-600^{o}C	●+	●$_{6009}$	●+	◊	◊	◊	◊	◊	◊
1-159s1	Base-700^{o}C	●+	●$_{2201}$+	◊	◊	◊	◊±	●$_{2424}$	●$_{2195}$	◊

For Sample 2 (10 min) are recorded the same phases but SnS is in other structure configuration [1:01-073-1859] in addition with ZnS [1:01-089-2347&00-012-0688]. Sample 3 (15min) is common for all other RTP configurations and consisted only of Kesterite and Hexagonal ZnS [1:01-089-2201, 01-089-2424& 01-089-2195].

On the next Figure 3 are presented Raman spectra of the same films. In accordance of [16–18] could be concluded that the spectra are dominated again of signals for Kesterite at 338, 287, 252, 374 and 97 cm^{-1}. After [19,20] disposition of the shoulder near 350 cm^{-1} in conjunction with signals at 98 cm-1 and possibly near 160 cm-1 could give an idea for the distribution of ZnS. On the same way the shift at 164 cm^{-1} and shoulder near 311cm^{-1} could be recognized as confirmation for presence of SnS

[21–23]. Vibration at 476 cm^{-1} is characteristic for the bong Cu-S in nonstoichiometric unsaturated copper sulphides [20]. This comparative analysis confirms as possible suggested phase distribution but full identification passes through of more detailed view on the XRD patterns.

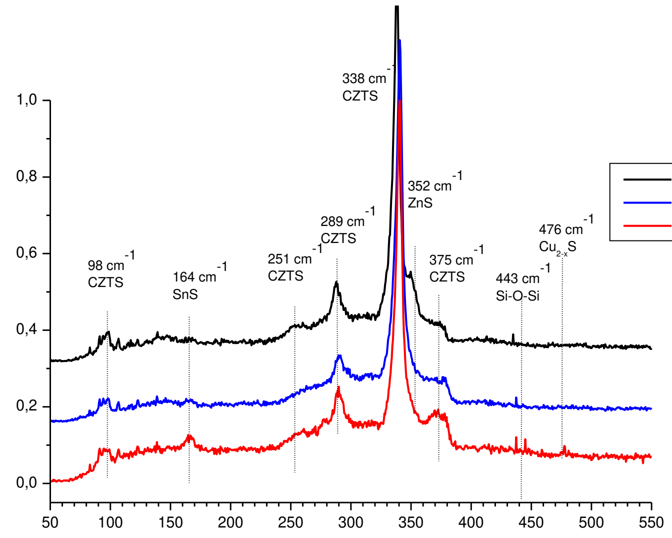

Figure 3. Raman shift – duration.

As was mentioned before the main phases in concomitant with the Kesterite dispose reflexes quite close to those for main phase but more precise analysis could reveal the fine structure of the films. At Figure 4 is presented part of pattern of Figure 2 in the vicinity of 13.0 – 14.0 ° 2Θ. The picture presents fine disposition of reflexes which allowed to distinguish the one for ZnS at 13.35° (Sample 3) from the other at 13.28° (Sample 2) belonging to Cu_7S_4.

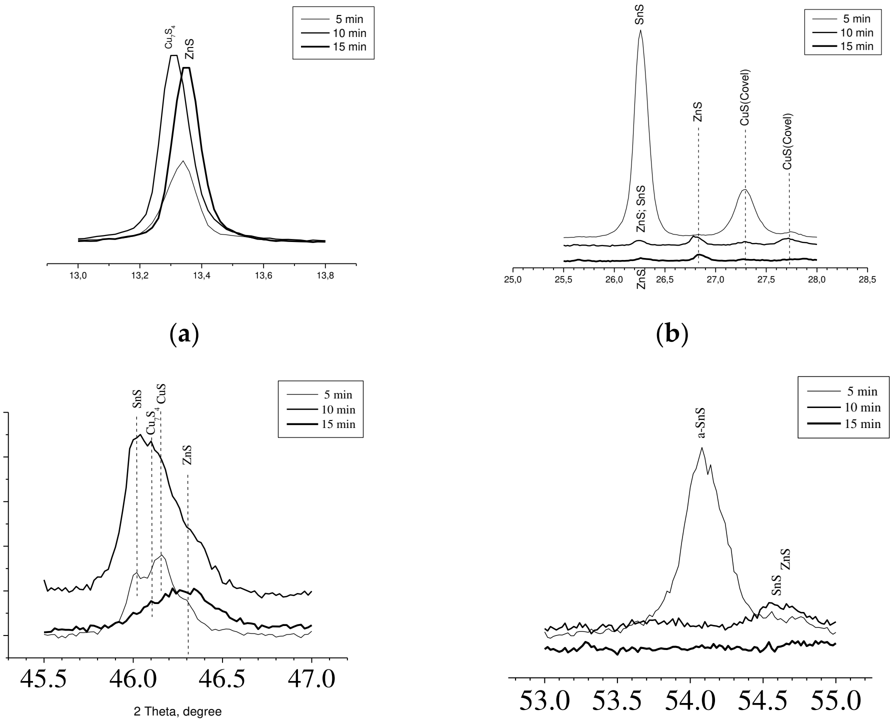

(**a**)

(**b**)

(**c**)

(**d**)

Figure 4. Pattern sections from Figure 2. **(a)** Pattern at 13.0 – 14.0 ° 2Θ.**(b)** Pattern at 25.5° – 28.0° 2Θ. **(c)** disposed pattern between angles 45.5°– 47.0°. **(d)** Pattern at 54°.

On Figure 4(b) is presented pattern from Figure 2 at the interval of 25.5° - 28.0° 2Θ. In accordance of performed phase recognition the reflex at 26.24° for Sample 1 should be assumed of coming from SnS only, for Sample 3 the small reflex at the same angle should be assumed of ZnS only but for Sample 2 the reflex should be consistent of ZnS and SnS.

At 26.82° are disposed reflexes only for Samples 2 and 3, recognized as from ZnS whereas at 27.28° and 27.75° are seen single signals from CuS for Samples 1 and 2. Further at Figure 4(c) are disposed pattern between angles 45.5°– 47.0°. Here the large signal from Sample 3 is due to ZnS. For Samples 1 and 2 the reflex at 46.02° is proving for SnS whereas those at 46.11° and 46.18° are caused of Cu_7S_4 and CuS respectively.

Figure 4(d) shows in details the field near 54°. The reflex at 54.05° for Sample 1 comes from α-SnS [1:01-083-1758] whereas from Sample 2 the reflex at 54.5° is due to SnS [1:01-073-1859] accompanied with Wurtzite [1:00-012-0688].

On Figure 5(a) are shown XRD patterns for Sample 4 (fast) and Sample 5(slow) that on comparison with Sample 1(base) present RTP configuration with different speeds of rising and decreasing of temperature for the dynamic Segments No2, No4, No6 and No8 (see Figure 1).

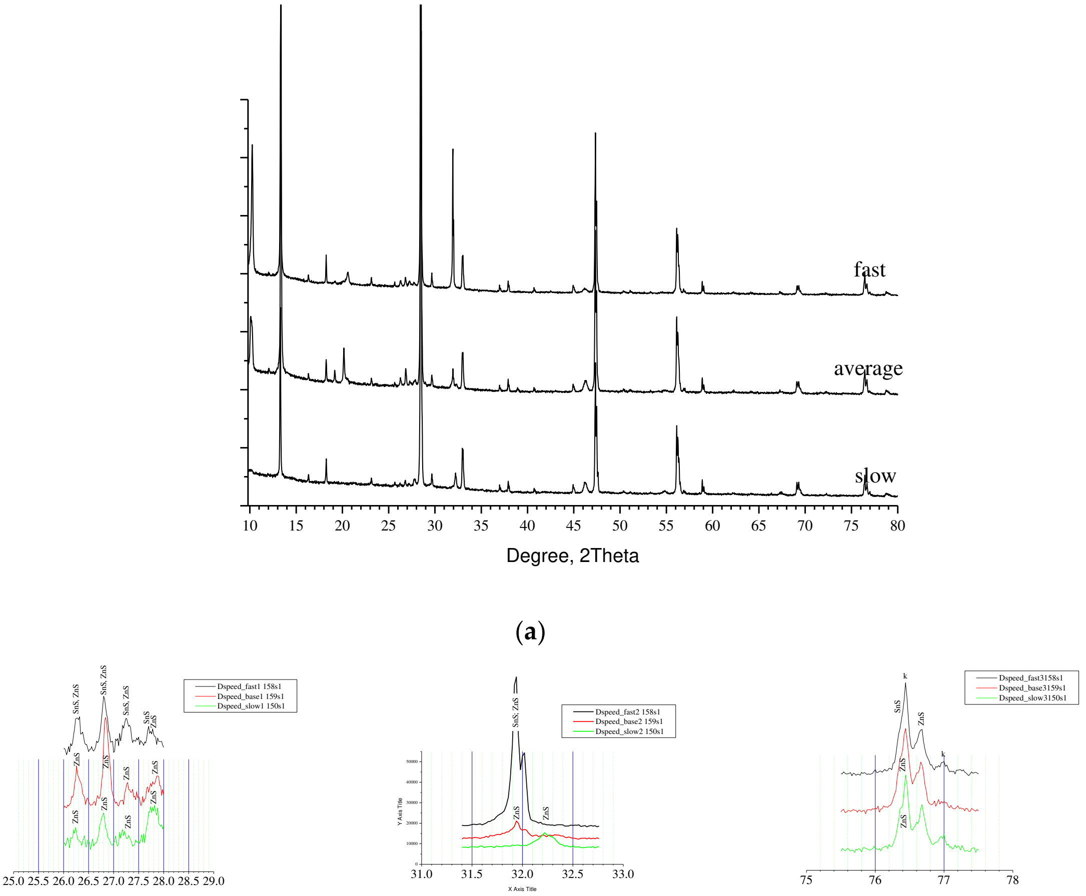

(**a**)

(**b**) (**c**) (**d**)

Figure 5. XRD patterns of samples annealed at different speed (see Figure 1 - Segments No:2,4,6 &8). **(a)** Superimposed diagram of all speeds. **(b)** Pattern in vicinity of 26° – 28° 2Θ. **(c)** Pattern in vicinity of 31.5° – 32.5°. **(d)** Pattern in vicinity of 76° –77°.

According to [21] phase distribution of the samples is summarised at Table 2. Sample 4, annealed at higher speed of rising of temperature contains mainly of Kesterite but pair of SnS phases – orthorhombic [1:01-072-8499] and [1:00-001-0984] is registered as well as a Hexagonal ZnS [1:01-074-

4998]. For Sample 5, annealed at slow rate are found Kesterite and Hexagonal ZnS [1:01-075-6022]. As was mentioned before the average rate Sample 1 contained Kesterite and Hexagonal zinc sulphides. Comparative phase analysis has shown the Kesterite and zinc sulphides as common structures in the three samples whereas Sample 4 contained in addition two forms of Herzenbergite [1:01-072-8499& 00-001-0984]. They have similar layered orthorhombic structure and differ in orientation. Obviously both of them are result of non-equilibrium interaction in the chain of formation of CZTS caused by the high speed of change of the temperature. Apparently, in more soft conditions - as longer reaction time (previous case) or slower dynamic parameters of the process, according with [22] this intermediate interact further on related scheme. On Figure 5(b) are shown XRD pattern of the samples in vicinity of 26 ° up to 28 ° 2Θ. Reflexes near 26.2 ° are assumed for all samples to be from ZnS but for Sample 4 it appears to be in convolution with signal from SnS. On the same way could be spell out the reflexes at 26.8 ° and at 27.3 °. Near 27.75 ° the disposition is quite similar but the complex reflex for Sample 4 looks well divided for both SnS and ZnS. On the next Figure 5(c) is presented interval 31.5 ° - 32.5 °. Sample 5 disposes here an individual reflex at 32.23 ° whereas the other Samples 1 and 4 present similar twin reflex at 31.94 ° and 32.02 °. [21] spelt out the twin for Sample 1 as came from ZnS only while for Sample 4 assumed pair of ZnS and SnS. This could be explained with obvious difference in the height (intensity) of the reflexes. Between 76 ° and 77 ° on Figure 5(d) are disposed reflexes at 74.4 ° and 77 ° assumed of Kesterite. ZnS is presented here with reflex at 76.68 ° and a shoulder at the first Kesterite reflex. For Sample 4 is distinguished here a twin shoulder caused of both ZnS and SnS. Raman spectra presented at Figure 6 are in good agreement with the supposed phase composition of the Samples 4,5 and 1. In all samples the Kesterite is well defined with the majority of its characteristic vibrations at 338 cm^{-1}, 289 cm^{-1}, 251 cm^{-1}, 98 cm^{-1} and 375 cm^{-1}. For all of samples is seen shoulder at 352 cm^{-1}, near the most intensive signal for Kesterite attributed to ZnS. Only for Sample 4 is registered resonant vibration at 164 cm^{-1}, attributed to SnS in confirmation with established XRD phase distribution.

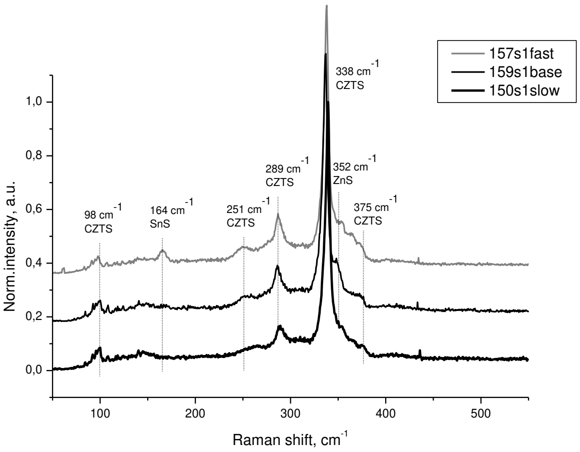

Figure 6. Raman shift for samples annealed at different speeds.

At the next Figure 7 is presented XRD pattern of Samples 6, 7 and 8 annealed in different temperature (level of Segment 5, Figure 1) respectively 600 °C, 650 °C and 750 °C which together with Sample 1 (700 °C for level of Segment 5) are the process set configuration for investigation of influence of the temperature. The Pattern present a well-crystallized Kesterite in all samples accompanied with different ZnS phases in almost the same structure [1:01-073-6009, 01-074-4989, 01-089-2201, 01-089-2424, 01-089-2195, 01-089-2140].

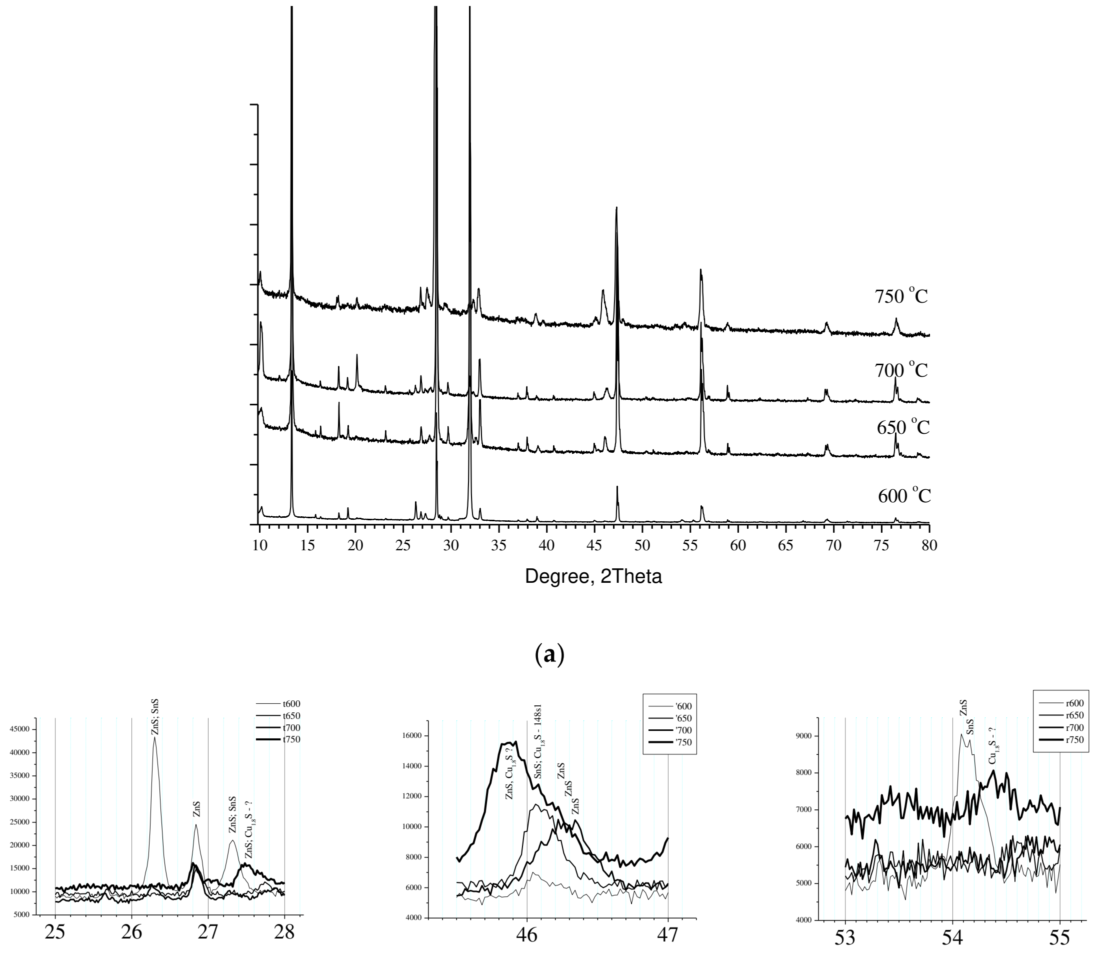

(**a**)

(**b**) (**c**) (**d**)

Figure 7. XRD patterns of Segment 5, RT-processed at different temperatures (see Figure 1.). **(a)** Superposition at different temperatures. **(b)** Pattern at 26 ° – 28 °. **(c)** 45.5 ° - 47 °. **(d)** 53 ° – 55 °.

For low temperature Samples 6 and 7, respectively annealed at 600 °C and 650 °C are registered hexagonal tin sulphides while for high temperature Sample 8 (750 °C) is attributed Digenite [1:01-070-9133]. Detailed XRD analysis at the interval 26 ° – 28 ° is shown at Figure 7(b). Sample 6 disposed three reflexes (at 26.30 °, 26.83 ° and 27.32 °) attributed to ZnS/SnS, ZnS and ZnS/SnS respectively. The reflex at 26.83 ° is common for the all samples whereas Sample 8 disposed a peak at 27.5 ° identified to ZnS and may be $Cu_{1.8}S$. On the next Figure 7(c) are shown interval of angles between 45.5 ° - 47 °. Samples 5 and 6 (600 °C and 650 °C) showed reflex at 46.08 ° recognized as caused from SnS. Between 46.2 ° and 46.4 ° is seen large reflex for Sample 1 attributed to ZnS. Sample 8 showed a peak between 45.80 ° and 45.82 ° attributable to ZnS and may be Digenite and a shoulder at 46.08 ° recognized as caused from SnS and may be Digenite. Further in Figure 7(d) at 53 ° - 55 ° Sample 5 (600 °C) disposed a twin at 54.09 ° and 54.16 ° whereas for Sample 8 (750 °C) at 54.38 ° was recognized a signal from Digenite.

On the next Figure 8 is presented set of pattern for Raman shift of the same samples. Raman spectra showed presence of Kesterite, ZnS and SnS for Sample 5 and Sample 6, Kesterite and ZnS for Sample 1 and Sample 8, but there were no seen confirmation for Cu-S bond. In sequence the features for phase composition recognized from XRD [21] analysis is confirmed by Raman shift, but only with exception of the phase $Cu_{1.8}S$. XRD reflexes for it was not defined uniquely and absence of specific Raman resonant vibration give reasons to consider this phase as non-existent.

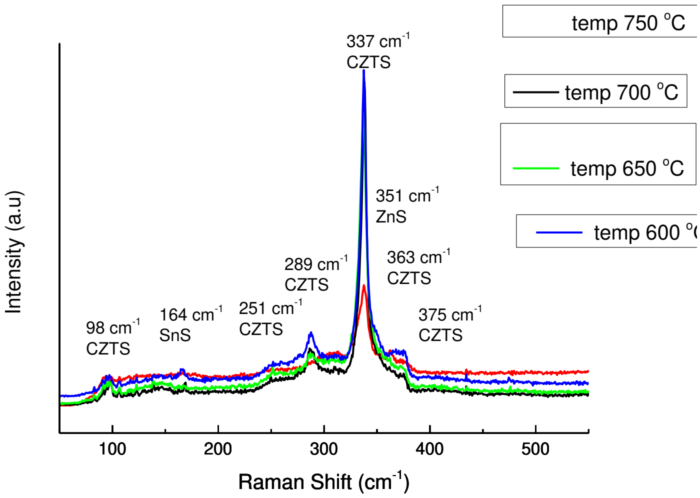

Figure 8. Raman shift for samples annealed at different speeds.

On the next Figure 9 are presented dependences of crystallite size and lattice strain, calculated by Williamson-Hall method [21] on dependence of process parameters for sets of investigating of influence of Duration of the Segment 5 (Samples 1, 2 and 3); Speed of change of temperature at dynamic segments 2, 4, 6 and 8 (Samples 4,1 and 5) and Temperature level of Segment 5 (Samples 6, 7, 1 and 8) respectively for 600 °C, 650 °C, 700 °C and 750 °C.

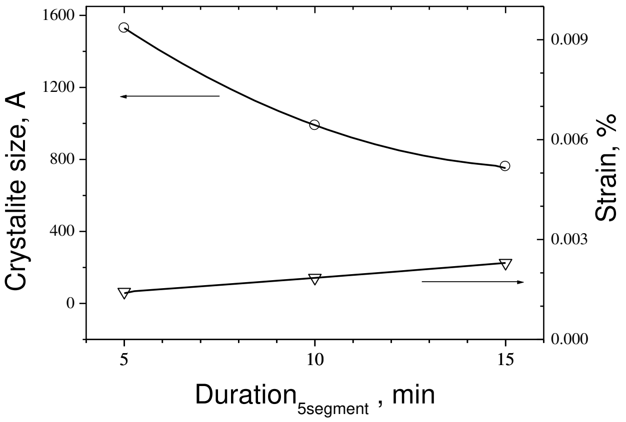

Figure 9. Crystallites size and strain of Kesterite formed by RTP at different duration.

As can be seen that the trend of crystallite size with rising of duration of Segment 5 from 5 to 15 min is decreasing from 1530 Å down to near 760 Å whereas the strain of the cell rises from 0.00143 % up to 0.00230 %. The same trend is seen for the temperature where the crystallite size drops from 1193 Å for 600 ºC to 609 Å for 750 ºC respectively and strain rises from 0.00133 % up to 0,0036 %.

For dependence of crystallite size and strain on the speed of change of the temperature the general trend is the same, but curves are not monotonous, as can be seen by Figure 10. The crystallite size is 1521 Å for the fast process and decrease down to 1010 Å for the slowest while at average speed is as low as 761 Å. The strain drops from 0.00139 % up to 0.00026 % while at average speed is at the maximum of 0,0023 %.

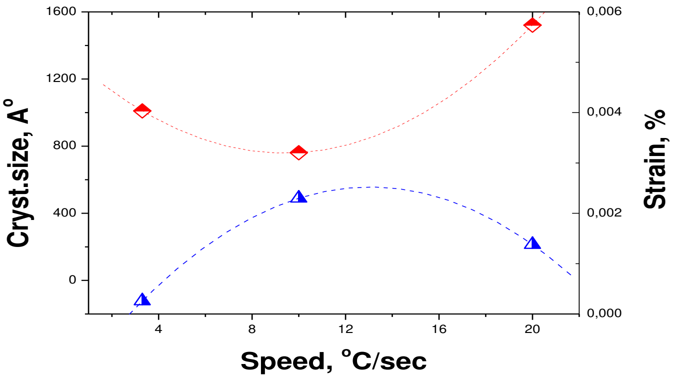

Figure 10. Crystallites size and strain of Kesterite formed by RTP at different speed.

Regarding the influence of temperature, as is shown in Figure 11, in comparison with the last data at [24-RenartCP] it is seen a remarkable difference. While the cell parameters for 700 °C at [24] are respectively a=5.6177 Å and c = 11.2232 Å in our case they are a = 5.4262 Å and c=10.8519 Å. This is the reason in consequence to register a difference in the cell volume at 600 °C from 335 Å^3[24] whereas cell volume in our case is near 320 Å^3.

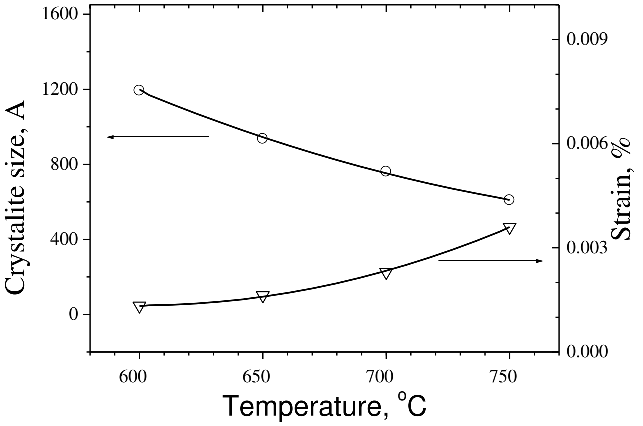

Figure 11. Crystallite size and strain for Kesterite phase formed by RTP at different temperatures.

Generally, could be concluded that slower and longer process at higher temperatures give from copper-poor zinc-rich near stoichiometric substrates a preferable phase composition of Kesterite and zinc sulphides, whereas the cell strain increase with rise of temperature and increase of duration of Segment 5, but decreases when the speed of the process decrease. Results are in agreement with [25] and the older one [26] but in some details are quite different from the newer works [24]. For example, the shown difference in cell parameters [24] at 700 °C is easy to explain having in mind the dynamic of the process – at [24] the process is near the equilibrium whereas in our case we demonstrate time resolved (faster) process which in slower stages coincides with previous results [24–26].

Figure 12 presents SEM micrographs of samples, annealed in different duration.

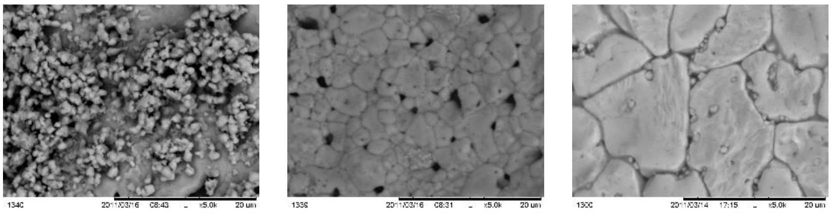

(**a**) (**b**) (**c**)

Figure 12. SEM footprints of samples, annealed at different time (Segment 5, Figure 1): **(a)** – 5 min; **(b)** – 10 min; **(c)** – 15 min.

For short time of annealing small part of as deposited layer crystallized on the substrate area, leaving un-reacted mass on the top surface. For 10 min (Figure 12 b) is formed pin-hols layer with grains sized between 1 – 4 µm whereas at 15 min (Figure 12 c) the grains are much larger sizing 4 - 5 µm at thickness near 1 µm.

Figure 13 presents morphology issues for samples annealed at different speed. It is seen enlarging of grain sizes from 1-2 µm for fast (Figure 13 a) annealing through 4-5 µm for average (Figure 13 b) going up to 8 – 10 µm for samples annealed at slow process (Figure 13 c).

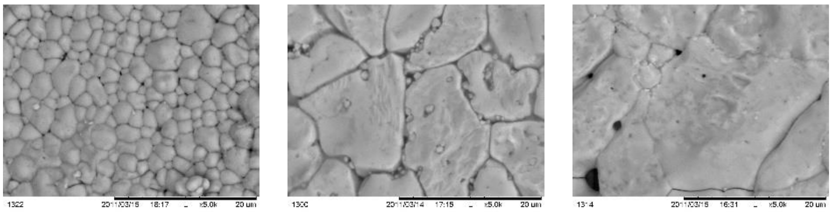

(**a**) (**b**) (**c**)

Figure 13. SEM fingerprints of samples RTAnnealed at different speed: a-fast process, b-average speed; c – slow process.

Figure 14 shows footprints of morphology for samples processed at different temperature. Figure 14(a) presents CZTS layer with single independent grains with size near 1 – 2 µm. At temperature 650 °C surface concentration of the grains raised and pinholes are seen as well. At 700 °C the grain sizes reach maximum 4-5 µm while at higher temperature 750 ºC got smaller with heterogeneous residuals on the grain borders.

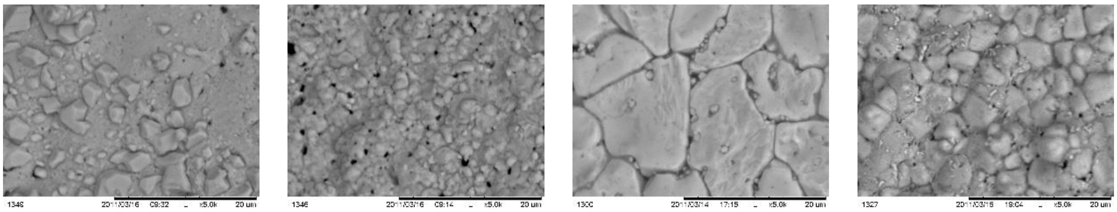

(**a**) (**b**) (**c**) (**d**)

Figure 14. SEM micrographs for samples annealed at different temperature: **(a)** – 600 °C; **(b)** – 650 °C; **(c)** - 700 °C and **(d)** – 750 °C.

SEM observations gave slightly different imagination for the crystallite size from the values, calculated. Figure 9 , Figure 10 and Figure 11 shows, derived from XRD analysis, crystallites sizes from 0.05 up to 0.15 µm whereas SEM present sizes near 1 – 8 µm at thickness near 1 µm.

Here we can conclude that tendences for change of the crystallite sizes, derived by XRD data by Williamson-Hall method [1-arvo] differs by an order of magnitude and in addition, are opposite of the tendences of change of grain sizes, derived by SEM. In fact, Williamson-Hall method gives sizes of short-ordered crystal unit of the Kesterite that is quite different from the visible grain structure of the layers.

As was reported elsewhere [RTAJScrag2012 and CZTS2014], the Raman spectroscopy could be used for characterizing of Cu/Zn disorders and distinguish the origin of the substitution in slow-cooled Kesterite thin films. Here is present a rough idea about dependences in time resolved RTA process.

On Figure 15(a) are presented dependences of Q and Q′ on the duration of the high-temperature annealing step of the process. It is seen that the both Q and Q′ increase with increasing of the duration. The order of magnitudes of increase of the Q is quite small – from 1.39 through 1.5 up to 1.86, whereas the Q′ is quite higher and increases near twice from 2.9 up to 4.7. The same trend is observed at the dependence of Q and Q′ on the temperature (level of segment 5), but at higher level of 750 °C the both Q and Q′ drops sharply. This effect could be interpreted as an increase in the disorder in the Kesterite structure. The increase of the speed of the increase and decrease of the temperature influence in opposite way the Q and Q′. This effect could be explained with increase in the disorder of the structure at high speed in the dynamic stages bringing the process closer to the case of quenching in the experiments in [CZTS2014].

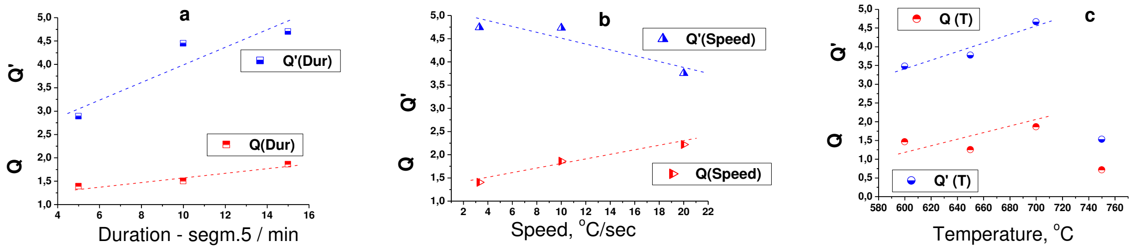

(**a**) (**b**) (**c**)

Figure 15. Dependences of Raman peaks ratios Q = I_{287}/I_{303} and Q′ = $I_{338}/(I_{366}+I_{374})$ on the RTA process parameters: **(a)** – duration of the segment 5; **(b)** – speed of the change of the temperature in the dynamic steps – segments 2,4 and 6; and **(c)** – temperature of the segment 4 (see Table 1).

5. Conclusions

Time resolved annealing process for CZTS thin films is performed. The peculiarities of phase composition and structure parameters of so formed thin Kesterite layers in dependence of process parameters (as time, speed and temperature) are analysed. Have been shown that phase composition of the layers depends on time and speed of the stage of formation of the Kesterite. At short time unreacted binary residuals as both copper sulphides and tin sulphides left. The dependence is the same for fast process where the dynamic change of the temperature gave not ability of binary reaction precursors to react up to the quaternary compound. For slow and long enough (at least 15 min in our case) processes low temperature binary precursors, according (schurr et al) react fully and only Kesterite and the high temperature ZnS left. Situation is the same regarding the temperature of the process of formation of CZTS. At low temperatures are registered un reacted binary copper and tin sulphides whereas at high temperatures (700 – 750 °C) is formed well crystallised Kesterite with immersions of ZnS, which is favourable phase composition regarding of properties of the photovoltaic properties of absorbers films. On the other side time dependent properties of the Kesterite are elucidated. It is shown that crystallites size decrease with increasing of the time of CZTS synthesis stage of the process. On the same way the strain in the cell rises. Generally, the same trend is observed for the process performed at different speed – for fast process the crystallites size is comparatively high and decrease with decreasing of the speed whereas the strain rises. When the temperature raises the crystallites size decreases, which is in formal contradiction with [14-Schurr et al]. But whereas [14-Schurr et al] lead the reactions near the equilibrium and it is reasonable to register well crystallised phases, time resolved process gives shorter time for equilibrium disposition of the atoms in the structure and formation of the phase appears in non-equilibrium condition. As consequence the strain in the crystal cell has gone up. The general trends evolved from the features of the RTP are better crystallization we have at longer and slower process at comparatively lower temperatures. But RTA favours extremely the thermal budget of thin absorber films processing and an appropriate optimisation will raise sharply the cost-efficiency ratio.

Acknowledgments: The part of the works was performed on equipment of Research Infrastructure “Energy Storage and Hydrogen Energetics” (ESHER), included in the National Roadmap for Research Infrastructure 2017-2023”, approved by DCM # 354 from 2017 and granted by the Ministry of Education and Science of Republic Bulgaria. The authors are thankful of COST Action 21148 ReNEW PV, Bilateral programs between Bulgarian

Academy of Sciences and Estonian Academy of Sciences – 2017 - 2020 and European researcher's mobility program of Estonian National Science Foundation under the Contract JD 98.

References

1. Woodhouse, Michael, Rebecca Jones-Albertus, David Feldman, Ran Fu, Kelsey Horowitz, Donald Chung, Dirk Jordan, and Sarah Kurtz. On the Path to SunShot: The Role of Advancements in Solar Photovoltaic Efficiency, Reliability, and Costs. *Golden, CO: National Renewable Energy Laboratory*. **2016,** NREL/TP-6A20-65872. http://www.nrel.gov/docs/fy16osti/65872.pdf.
2. Richter, A.; Hermle, M.; Glunz, S.W. Reassessment of the Limiting Eciency for Crystalline Silicon Solar Cells. *IEEE J. Photovolt*. **2013**, *3*, 1184–1191
3. Yoshikawa, K.; Hayato, K.; Wataru, Y.; Toru, I.; Katsunori, K.; Kunihiro, N.; Toshihiko, U.; Daisuke, A.;Masanori, K.; Hisashi, U.; et al. Silicon heterojunction solar cell with interdigitated back contacts for a photoconversion efficiency over 26%. *Nat. Energy* **2017**, *2*, 17032
4. M. Nakamura, K. Yamaguchi, Y. Kimoto, Y. Yasaki, T. Kato, H. Sugimoto, Cd-Free Cu(In, Ga)(Se, S)2 Thin-Film Solar Cell With Record Efficiency of 23.35%, *IEEE J. Photovoltaics*, **2019,** *9 (6)*, pp. 1863-1867, 10.1109/JPHOTOV.2019.2937218
5. S.R.I. Biplab, M.H. Ali, M.M.A. Moon, M.F. Pervez, M.F. Rahman, J. Hossain, Performance enhancement of CIGS-based solar cells by incorporating an ultrathin BaSi2 BSF layer, *J. Comput. Electron*., **2020,** *19 (1)* pp. 342-352, 10.1007/s10825-019-01433-0
6. M.P.Paranthman, W.Wong-Ng, R.N.Bhattacharya, Semiconductor materials for solar photovoltaic cells, *Springer*, **2016**, ISBN: 978-3-319-20331-7
7. Hironori Katagiri, Nobuyuki Sasaguchi, Shima Hando, Suguro Hoshino, Jiro Ohashi, Takaharu Yokota, Preparation and evaluation of Cu2ZnSnS4 thin films by sulfurization of E-B evaporated precursors, *Solar Energy Materials and Solar Cells*, **1997,** *Volume 49, Issues 1–4,* Pages 407-414, https://doi.org/10.1016/S0927-0248(97)00119-0
8. Ingrid L. Repins; Manuel J. Romero; Jian V. Li; Su-Huai Wei; Darius Kuciauskas; Chun-Sheng Jiang; Carolyn Beall; Clay DeHart, "Kesterite Successes, Ongoing Work, and Challenges: A Perspective From Vacuum Deposition", *IEEE Journal of Photovoltaics*, **2013,** *vol. 3, no. 1*, pp. 439-445, doi: 10.1109/JPHOTOV.2012.2215842.
9. Wang,W.;Winkler, M.T.; Gunawan, O.; Gokmen, T.; Todorov, T.K.; Zhu, Y.; Mitzi, D.B. Device Characteristics of CZTSSe Thin-Film Solar Cells with 12.6% Efficiency. *Adv. Energy Mater*. **2014**, *4*, 1301465.
10. Yaroslav E Romanyuk, Stefan G Haass, Sergio Giraldo, Marcel Placidi, Devendra Tiwari, David J Fermin, Xiaojing Hao, Hao Xin, Thomas Schnabel, Marit Kauk-Kuusik, Paul Pistor, Stener Lie and Lydia H Wong. Doping and alloying of kesterites, *Journal of Physics: Energy*, **2019,** *Volume 1, Number 4*, DOI 10.1088/2515-7655/ab23bc
11. International Center for Diffraction Data: Available Online: https://www.icdd.com/
12. R. Schurr, A. Hölzing, S. Jost, R. Hock, T. Voß, J. Schulze, A. Kirbs, A. Ennaoui, M.Lux-Steiner, A. Weber, I. Kotschau, H.-W. Schock, The crystallisation of Cu_2ZnSnS_4 thin film solar cell absorbers from coelectroplated Cu-Zn-Sn precursors, *Thin Solid Films*, **2009**, *517*, pp 2465–2468.
13. P.M.P. Salomé, P.A. Fernandez, A.F. da Cunha, Morphological and structural characterization of $Cu_2ZnSnSe_4$ thin films grown by selenization of elemental precursor layers, *Thin Solid Films*, **2009**, *517*, pp 2531–2534.
14. M. Ganchev, J.Iljina, L.Kaupmees, T.Raadik, O.Volobujeva, M.Altosaar, A.Mere, J.Raudoja, E.Mellikov. Phase composition of selenized Cu2ZnSnSe4 thin films determined by X-ray diffraction and Raman spectroscopy, *Thin Solid Films*, **2011**, *Volume 519, Issue 21*, pp. 7394-7398, doi:10.1016/j.tsf.2011.01.388
15. P.A. Fernandes, P.M.P. Salomé, A.F. da Cunha, Growth and Raman scattering characterization of Cu2ZnSnS4 thin films, *Thin Solid Films*, **2009**, *517*, pp. 2519–2523
16. M. Himmrich and H. Haeuseler, LATTICE VIBRATION-SPECTRA Spectrochim. Acta A, *Mol. Spectrosc.*, **1991**, *47*, 933.
17. M. Altosaar, J. Raudoja, K. Timmo, M. Danilson, M. Grossberg, J. Krustok, E. Mellikov. $Cu_2Zn_{1-x}Cd_x Sn(Se_{1-y} S_y)_4$ solid solutions as absorber materials for solar cells, *Phys. Stat. Sol(a)*, **2008**, *205*, 167
18. M. Grossberg, J. Krustok, J. Raudoja, K. Timmo, M. Altosaar, T. Raadik, Photoluminescence and Raman study of $Cu_2ZnSn(Se_xS_{1-x})_4$ monograins for photovoltaic applications.*Thin Solid Films*, **2010**, doi:10.1016/j.tsf.2010.12.099
19. Young-Moon Yu, M.-H. Hyun, S. Nam, D. Lee, O. Byungsung, K.- S. Lee, Pyeong Yeol Yu, Yong Dae Choi, *J. Appl. Phys.*, **2002**, *91*, pp. 9429.
20. P. A. Fernandes, P. M. P. Salome and A. F. da Cunha, A study of ternary Cu_2SnS_3 and Cu_3SnS_4 thin films prepared by sulfurizing stackedmetal precursors. *J. Phys. D: Appl. Phys.*, **2010**, *43*, 215403
21. L.S. Price, I.P. Parkin, A.M.E. Hardy, R.J.H. Clark, T.G. Hibbert and K.C. Molloy, Atmospheric Pressure Chemical Vapor Deposition of Tin Sulfides (SnS, Sn_2S_3, and SnS_2) on Glass. *Chem. Mater*, **1999**, *11*, pp. 1792-1799

22. H. R. Chandrasekhar, R.G. Humphreys, U. Zwick, M. Cardona, Infrared and Raman spectra of the IV-VI compounds SnS and SnS2. *Phys. Rev. B*, **1977**, *15*, 2177
23. Mare Altosaar, unpublished results.
24. Susan Schorr, Alfons Weber, Veijo Honkimäki , Hans-Werner Schock, In-situ investigation of the kesterite formation from binary and ternary sulphides, *Thin Solid Films*, **2009**, *517*, pp. 2461–2464
25. Hironori Katagiri, Nobuyuki Sasaguchi, Shima Hando,Suguru Hoshino, Jiro Ohashi, Takaharu Yokota, Preparation and evaluation of Cu_2ZnSnS_4 thin films by sulfurization of E-B evaporated precursors, *Solar Energy Materials and Solar Cells*, **1997**, *49*, pp. 407-414
26. W. Schiller, R. Nitsche, *Mater. Res. Bull.*, **1974**, *9*, pp. 645.